Electronic Supporting Information

$K_5[B_3O_3F_4(OH)]_2(NO_3)$: the first hydroxyfluorooxoborate-nitrate with short ultraviolet cutoff edge and large birefringence

Luyong Zhang,[a,b] Shibin Wang,[a] Fangfang Zhang,[a,b] Zhihua Yang,[a,b] and Xueling Hou *[a,b]*

[a]Research Center for Crystal Materials; CAS Key Laboratory of Functional Materials and Devices for Special Environments; Xinjiang Technical Institute of Physics and Chemistry, CAS, 40-1 South Beijing Road, Urumqi 830011, China.

[b]Center of Materials Science and Optoelectronics Engineering, University of Chinese Academy of Sciences, Beijing 100049, China.

[*]Corresponding authors, Emails: ffzhang@ms.xjb.ac.cn, xlhou@ms.xjb.ac.cn

CONTENTS

1. Experimental Section

Reagents

H_3BO_3 (Aladdin, 99.99 %), KF (Aladdin, 99.9 %), KNO_3 (Aladdin, 99.99 %), NH_4F (Aladdin, 99.99 %).

Crystals preparation. The crystals of $K_5[B_3O_3F_4(OH)]_2(NO_3)$ were obtained through the solution evaporation method. A mixture of H_3BO_3, KF, KNO_3, and NH_4F was weighed into a clear polypropylene beaker at a molar ratio of 6: 4: 1: 4. Then, 20 ml of distilled water was added to the beaker without further operation. Solvent water evaporated slowly at room temperature. Finally, the crystals were obtained. The single crystals were peeled off from the obtained crystals. And the polycrystalline powder samples were obtained by grinding the obtained crystals. The process of synthetic steps can be represented as the following chemical equation:

$$6H_3BO_3 + 4KF + KNO_3 + 4NH_4F \rightarrow K_5[B_3O_3F_4(OH)]_2(NO_3) + 10H_2O + 4NH_3$$

2. Characterizations

Structure determination. The crystal structure of the compound was collected by a Bruker D8 Venture single-crystal X-ray diffractometer with Mo-Kα radiation (λ = 0.71073 Å) at 273.15 K. During data collection, the cryogenic system of the instrument was invoked. The system would keep the test sample at a set temperature by spraying it with liquid nitrogen. Then the crystal structure was solved with the SHELXT structure solution program and refined with the SHELXTL crystallographic software package.[1] The program PLATON and the check CIF tool (http://checkcif.iucr.org) were used to check the crystal structure.[2] The relevant single-crystal information and final

refinements data, BVS calculations, and hydrogen bonds are given in Tables S1-S3. In particular, for the crystal structure analysis, the following content should be highlighted. The B1 is temporarily determined to be attached to three O atoms to form the [BO_2(OH)] group because the triple-coordinated B has not yet appeared to form [BO_2F]. Through elemental analysis, the Energy Dispersive X-ray spectrum confirms the presence of F in the crystal. Therefore, tetra-coordinated B atoms are temporarily determined to be attached to two O atoms and two F atoms to form the [BO_2F_2] groups. Furthermore, in conjunction with the Nuclear Magnetic Resonance spectra, the four peaks at -128.6899, -132.7783, -137.9142 and -142.2403 ppm can be assigned to B–F bonds, and the presence of the B–F bonds for the [BO_2F_2] groups can be proved by the $^{11}B\{^{19}F\}$-REDOR spectrum.

Powder X-ray diffraction (XRD). Powder XRD measurement data of the polycrystalline powder of the compound was collected by a Bruker D2 PHASER X-ray diffractometer with Cu Kα radiation (λ = 1.5418 Å). The diffraction pattern was taken with a scan step width of 0.02 ° and a fixed counting time of 2 s·step^{-1}. The XRD pattern of the polycrystalline powder sample of the compound agrees with the calculated result. The comparison of powder XRD data in terms of experimental and simulated patterns is given in a typical Rietveld-style difference plot, which can further verify the purity of the pure phase. And the full Rietveld refinement was performed by using the GSAS-II software, as shown in Figure S4.[3]

Elemental analysis. Energy dispersive X-ray (EDX) spectrum was measured on a SUPRA 55VP field emission scanning electron microscope equipped with a BRUKER

X-ray Flash-SDD-5010 energy-dispersive X-ray spectroscope.

Infrared (IR) spectroscopy. The IR spectrum of $K_5[B_3O_3F_4(OH)]_2(NO_3)$ was recorded by the ATR attachment of a Shimadzu IR Affinity-1Fourier transform IR spectrometer in the range of 400-4000 cm^{-1}. The sample was mixed with KBr in a mass ratio of 1 (polycrystalline powder sample): 100 (KBr).

Solid-State Magic Angle Spinning (MAS) Nuclear Magnetic Resonance (NMR). The polycrystalline powder of $K_5[B_3O_3F_4(OH)]_2(NO_3)$ was characterized by solid-state MAS NMR, which were performed on a Bruker Avance III 500 WB (11.75 T) spectrometer operating at a frequency of 470.96 and 160.61 MHz for 19F and 11B, respectively. The instrument equipped with a DVT quadruple resonance H/F/X/Y 2.5 mm CP/MAS probe was used with a spinning frequency of 30.0 kHz. PTFE, abound with CF_2 groups, was used as the external reference of ^{19}F chemical shifts, while boric acid solution at a specific concentration ($1 mol \cdot L^{-1}$), was utilized as an external reference for ^{11}B chemical shifts. Solid-state ^{19}F MAS NMR spectrum was recorded with a single pulse excitation using a 90 ° pulse width of 1.9 μs ($\frac{\pi}{2}$) and a recycle delay of 5 s to obtain quantitative results. Solid-state ^{11}B MAS NMR spectrum was recorded with a single pulse excitation using a short pulse length (0.32 μs) and a recycle delay of 10 s (the tip angle was $\frac{\pi}{12}$) to obtain quantitative results. Solid-state ^{1}H MAS NMR spectrum was recorded with a single pulse excitation using a 90 ° pulse length of 3.4 μs and a recycle delay of 4 s to obtain quantitative results. Meanwhile, the existence of B-F bonds was checked employing $^{11}B\{^{19}F\}$-REDOR MAS NMR spectroscopy.

Ultraviolet-visible-near infrared (UV-Vis-NIR) diffuse reflectance spectroscopy. The UV-Vis-NIR diffuse reflectance spectrum was measured with a Shimadzu SolidSpec-3700DUV spectrophotometer in the wavelength range of 200-2600 nm to determine the cutoff edge of $K_5[B_3O_3F_4(OH)]_2(NO_3)$. And the experimental bandgap was obtained from the absorption data which was transformed through the Kubelka-Munk function.

Thermal analysis. Thermal gravimetric (TG) analysis and differential scanning calorimetry (DSC) of the compound was carried out on a simultaneous NETZSCH STA 449C thermal analyzer instrument to evaluate the structural stability of the compound. The polycrystalline powder was put in a Pt crucible and heated at a rate of 5 °C min^{-1} in the range of 40-800 °C under a flow of N_2.

3. Calculation details

The theoretical calculation of $K_5[B_3O_3F_4(OH)]_2(NO_3)$ was performed by using the plane-wave pseudopotential approach of the CASTEP package.[4] The linear optical properties, electronic structures, and the density of states (DOS) of $K_5[B_3O_3F_4(OH)]_2(NO_3)$ were calculated via the density functional theory (DFT).[5] The Perdew-Burke-Ernzerhof (PBE) exchange-correlation of generalized gradient approximation (GGA) was used to optimize the exchange-correlation function.[6] Under the norm-conserving pseudopotential (NCP), the following orbital electrons were treated as valence electrons: H:$1s^1$, K-$3s^23p^64s^1$, B-$2s^22p^1$, N-$2s^22p^3$, O-$2s^22p^4$, and F-$2s^22p^5$. The value of the kinetic energy cutoff was set reasonably as 850.0 eV. Monkhorst-Pack *k*-point meshes (3 × 3 × 5) with a density of fewer than 0.025 $Å^{-1}$ were

used in the Brillouin zone, too. The default settings of the CASTEP code were utilized for additional calculation parameters and convergence criteria. Although the electronic structures of numerous crystals can be described by GGA-PBE, the discontinuity in exchange-correlation energy causes the calculated values that usually underestimate the experimental values. In order to simulate more accurately and obtain more reliable birefringence, the scissors correction was set to be 1.699 eV which was the distinction between the GGA calculation and the experimental band gap value originating from the transformation of the Kubelka-Munk function. Using the dielectric function $\varepsilon(\omega) = \varepsilon_1(\omega) + i\varepsilon_2(\omega)$, calculated the linear optical refractive indices of $K_5[B_3O_3F_4(OH)]_2(NO_3)$. And the imaginary part of $\varepsilon_2(\omega)$ was obtained from the equation:

$$\varepsilon_2\left(q \to O_{\hat{u}}, h\omega\right) = (2e^2\pi/\Omega\varepsilon_o) \sum_{kcv} \left|\left\langle \varphi_k^c | u \cdot r | \varphi_k^v \right\rangle\right|^2 \delta\left[E_k^c - E_k^v - E\right],$$

where h stands for Planck's constant, e stands for the elementary charge, r is the position operator, u stands for the vector which defines the incident polarization, Ω is the volume of the unit cell, ε_o is the dielectric constant, φ_k^v and φ_k^c represent the transition of momentum matrix element, E_k^c and E_k^v are used to represent energies of the occupied and unoccupied electronic states. Then, the birefringence Δn is determined by the real section of the dielectric function $\varepsilon_1(\omega)$ via the Kramers-Kronig transformation. The Response Electron Distribution Anisotropy Index (REDA) developed from the bond valence model can be used to analyze the contribution of different covalent groups to the linear optical response, *i.e.*, the REDA index which is proportional to the birefringence magnitude, and the specific relationship can be expressed by the

following equation:

$$\Delta n = \frac{R\sum_{g}[N_c Z_a \Delta\rho^b]_g}{2n_1 E_o},$$

where R is the correction coefficient, N_c is the coordination number of the nearest neighbor cations to the central anion, Z_a is the formal chemical valence of the anion and E_o is the optical bandgap, $\Delta\rho^b = \rho^b_{max} - \rho^b_{min}$, ρ^b_{max} and ρ^b_{min} are the maximum and minimum of the covalent electron density of the covalent bond on the optical principal axes of a crystal, and n_1 is the minimum refractive index. Within the same compound, the contribution of the groups to the birefringence is directly proportional to their respective $\Delta\rho$. Therefore, their contributions to the birefringence can be quantified by calculating and comparing the $\Delta\rho$ of each group.[7]

Table S1. Crystal data and structure refinement information of $K_5[B_3O_3F_4(OH)]_2(NO_3)$.

Empirical formula	$K_5[B_3O_3F_4(OH)]_2(NO_3)$
Formula weight	604.39
Temperature/K	273.15
Crystal system	Monoclinic
Space group	*C*2/*c*
a/Å	16.1792(9)
b/Å	13.4126(8)
c/Å	8.1449(6)
α/°	90
β/°	100.508(3)
γ/°	90
Volume/Å^3	1737.84(19)
Z	4
ρ_{calc} g/cm^3	2.310
μ/mm^{-1}	1.399
F(000)	1176.0
Crystal size/mm^3	0.149 × 0.112 × 0.075
Radiation (λ = 0.71073 Å)	Mo-Kα
Completeness (%)	99.9
2θ range for data collection/°	3.97 to 55.07 (0.77 Å)
Index ranges	$-20 \le h \le 20$, $-16 \le k \le 17$, $-10 \le l \le 10$
Reflections collected	9125
Independent reflections	2008 [R_{int} = 0.0599, R_{sigma} = 0.0448]
Data/restraints/parameters	2008/1/159
Goodness–of–fit on F^2	1.042
Final *R* indexes [$I \ge 2\sigma(I)$][a]	R_1 = 0.0344, wR_2 = 0.0651
Final *R* indexes [all data][a]	R_1 = 0.0543, wR_2 = 0.0733
Largest diff. peak/hole / e Å^{-3}	0.34/–0.33

[a] $R_1 = \Sigma||F_o| - |F_o||/\Sigma|F_o|$ and $wR_2 = [\Sigma w(F_o^2 - F_o^2)^2 / \Sigma wF_o^4]^{1/2}$ for $F_o^2 > 2\sigma(F_o^2)$

Table S2. Bond valence sum (BVS) calculations for $K_5[B_3O_3F_4(OH)]_2(NO_3)$.

Atom	BVS	Atom	BVS
K1	1.21	O4	2.07
K2	1.06	O5	1.91
K3	1.05	O6	2.03
B1	3.07	O7	1.95
B2	3.06	F1	1.08
B3	3.04	F2	0.86
N1	5.03	F3	1.04
O1	2.17	F4	1.02
O2	2.11	H1	1.05
O3	2.16		

Table S3. Hydrogen bonds for $K_5[B_3O_3F_4(OH)]_2(NO_3)$.

D	H	A	d(D-H)/Å	d(H-A)/Å	d(D-A)/Å	D-H-A/°
O1	H1	O5	0.931(10)	1.98(3)	2.731(6)	137(3)
O1	H1	O7	0.931(10)	2.003(15)	2.907(6)	163(3)

Table S4. Statistical results of inorganic hydroxyfluorooxoborates according to the Inorganic Crystal Structure Database (ICSD, with version 5.0.0, the latest release of ICSD-2023/01) and literature published in recent years.

No.	Compound	Space group	Birefringence	Ref.
1	$(NH_4)_4[B_{12}O_{16}F_4(OH)_4]$	*P*4/*ncc*	0.12 at 546 nm (exp.)	8
2	$LiB_5O_5F_2(OH)_4$	$P2_1/m$	0.124 at 546 nm (cal.)	9
3	$Na[B_3O_3F_2(OH)_2]\cdot[B(OH)_3]$	$P\bar{1}$	0.1252 at 546 nm (cal.)	10
4	$NaB_3O_4F(OH)$	$P2_1/c$	0.097 at 1064 nm (cal.)	11
5	$K_2[B_2O_2F_2(OH)_2]\cdot 2H_2O$	*	*	12
6	$(NH_4)_2[B_2O_2F_2(OH)_2]\cdot 2H_2O$	*	*	12
7	$K_2[B_3O_3F_4(OH)]$	*	*	13
8	$Cs[B_3O_3F_2(OH)_2]$	$P2_1/c$	0.049 at 1064 nm (cal.)	14
9	$Ba[B_2OF_3(OH)_2]_2$	*C*2/*m*	0.109 at 200 nm (cal.)	15
10	$(NH_4)_2[B_3O_3F_4(OH)]$	*C*2/*c*	0.049 at 1064 nm (cal.)	16
11	$Rb_2[B_3O_3F_4(OH)]$	*C*2/*c*	0.038 at 1064 nm (cal.)	16
12	$Cs_2[B_3O_3F_4(OH)]$	*C*2/*c*	0.035 at 1064 nm (cal.)	16
13	$Rb_2B_6O_9F(OH)$	*Cc*	0.05 at 1064 nm (cal.)	17
14	$Rb[B_3O_3F_2(OH)_2]$	*C*2/*m*	0.08 at 1064 nm (cal.)	18

* Unreported.

Table S5. Assignment of infrared absorption peaks for $K_5[B_3O_3F_4(OH)]_2(NO_3)$.

Vibration mode description of the characteristic absorption peak	Wavenumber (cm^{-1})
stretching vibration of O–H bonds	3418
stretching vibrations of N–O bonds	1443
asymmetric stretching vibrations of B–O bonds	1385
symmetric stretching vibrations of B–O bonds	953
bending vibrations of B–O bonds	802-467
symmetric out-of-phase stretching vibrations of B–F bonds	899
asymmetric stretching vibrations of B–F bonds	1177-1099

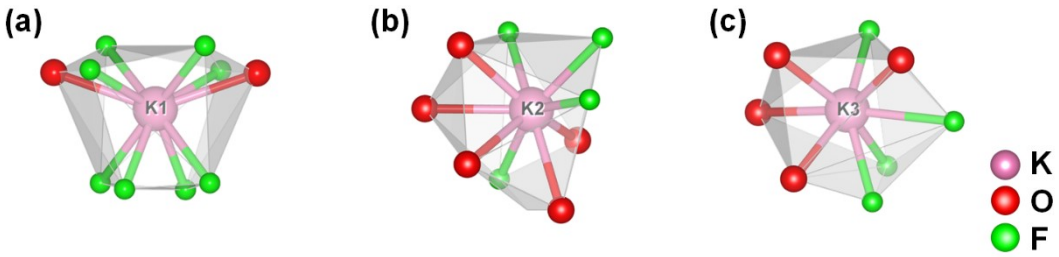

Figure S1. Coordination environment of (a) K1, (b) K2, and (c) K3 atoms.

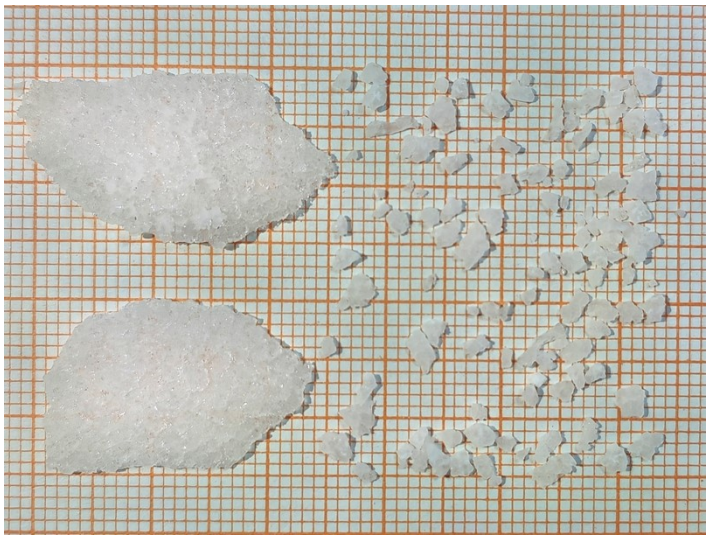

Figure S2. The photograph of $K_5[B_3O_3F_4(OH)]_2(NO_3)$ crystals.

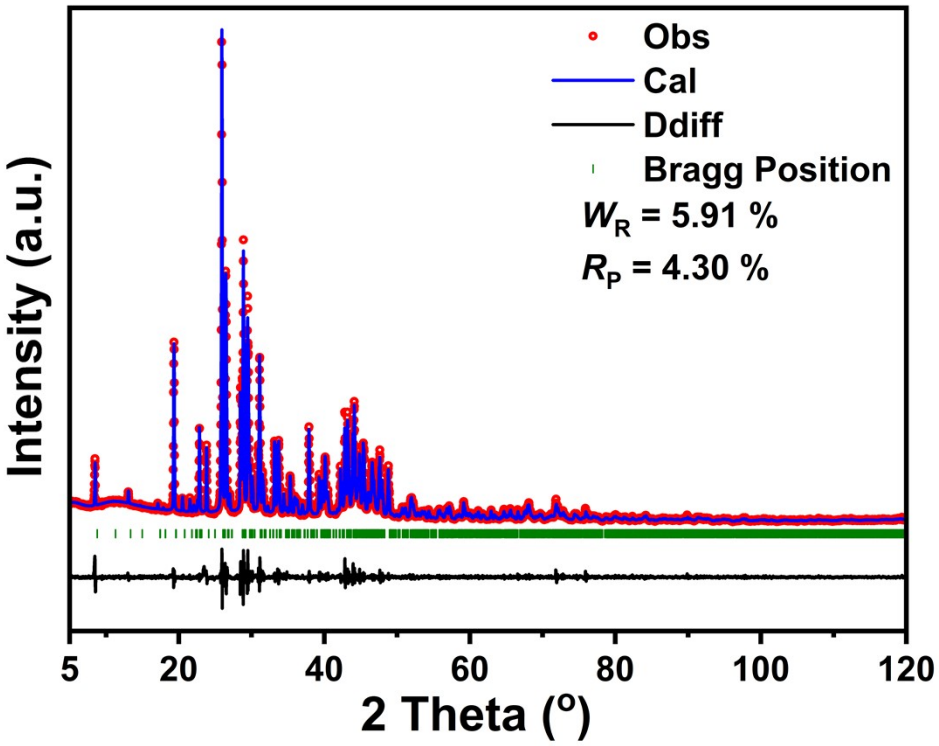

Figure S3. Rietveld refinement of the powder XRD profile of $K_5[B_3O_3F_4(OH)]_2(NO_3)$.

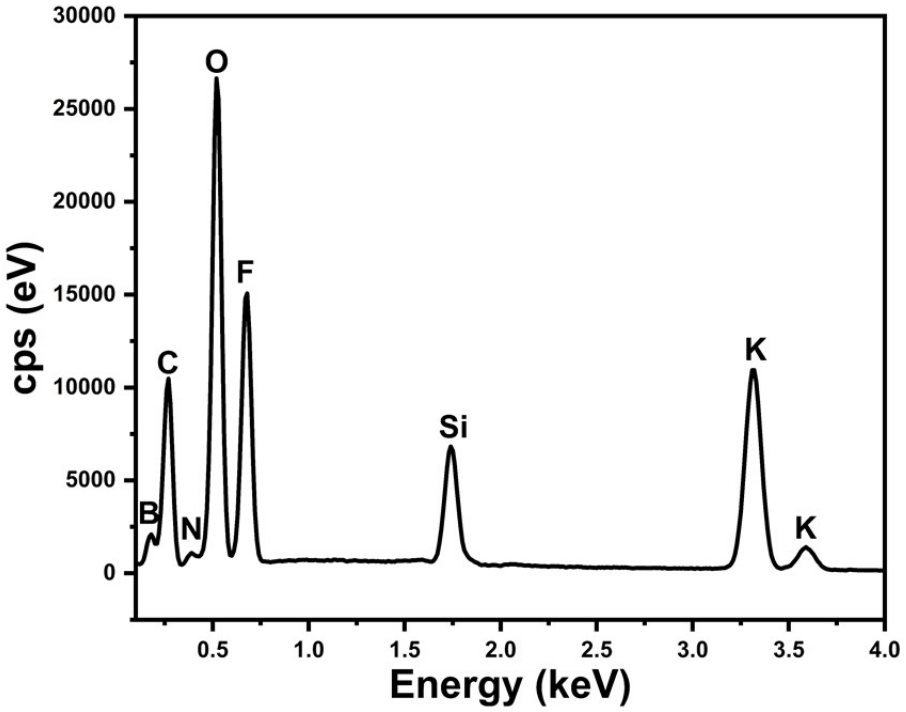

Figure S4. The EDX spectrum of $K_5[B_3O_3F_4(OH)]_2(NO_3)$. It was inevitable that C and Si would be detected since the sample tested was kept in dimethylsilicone oil.

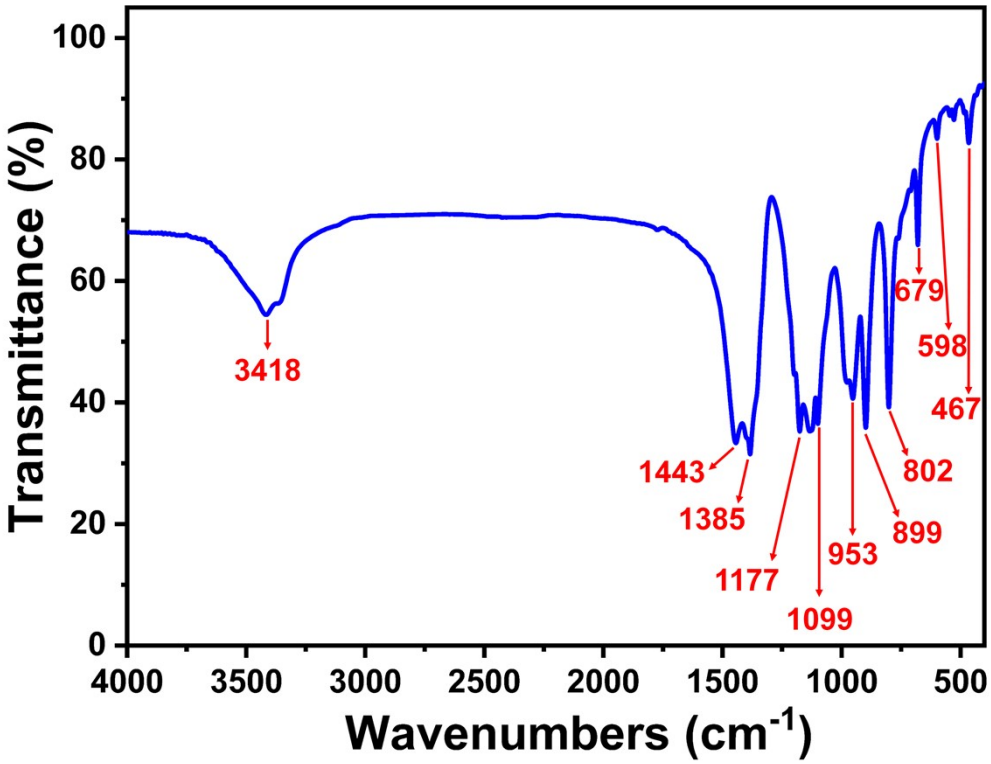

Figure S5. The infrared spectrum of $K_5[B_3O_3F_4(OH)]_2(NO_3)$.

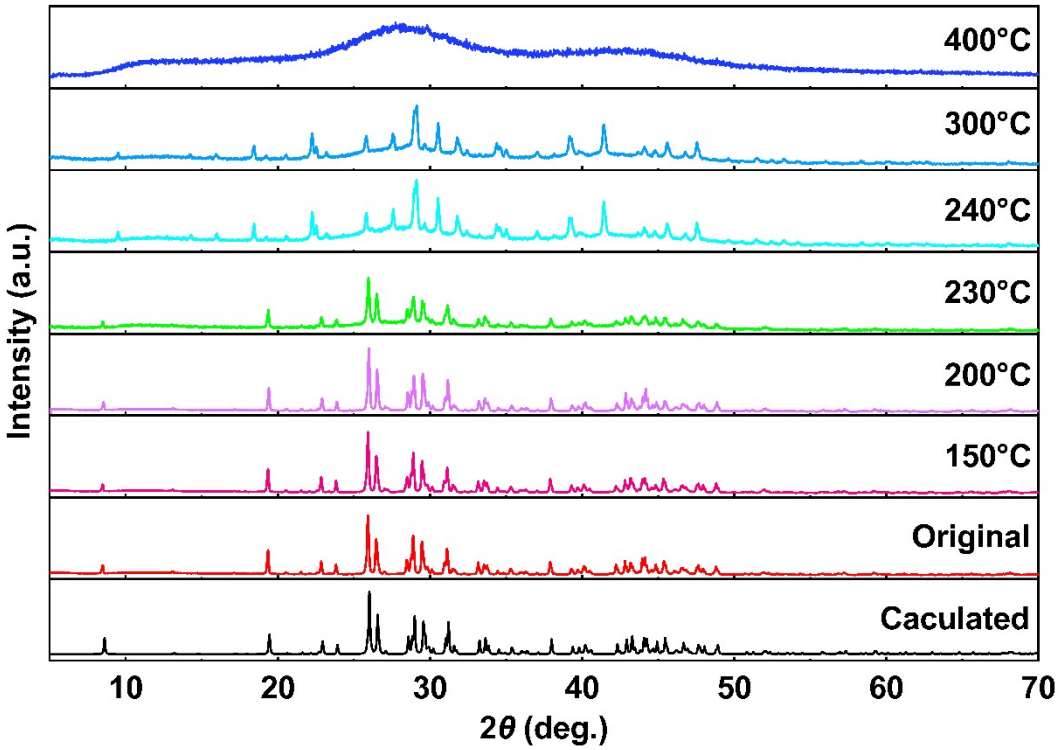

Figure S6. The calculated, original, and experimental XRD patterns of $K_5[B_3O_3F_4(OH)]_2(NO_3)$.

4. Reference

1 (a) SAINT, Version 7.60A, Bruker Analytical X-ray Instruments, Inc., Madison, WI, 2008; (b) O. V. Dolomanov, L. J. Bourhis, R. J. Gildea, J. A. Howard and H. Puschmann, *J. Appl. Crystallogr.*,2009, **42**, 339-341.

2 A. Spek, *J. Appl. Crystallogr.*, 2003, **36**, 7-13.

3 B. H. Toby, R. B. Von Dreele, *J. Appl. Crystallogr.*, 2013, **46**, 544-549.

4 S. J. Clark, M. D. Segall, C. J. Pickard, P. J. Hasnip, M. I. Probert, K. Refson and M. C. Payne, *Z. Kristallogr-Cryst. Mater.*, 2005, **220**, 567-570.

5 T. L. Gilbert, *Phys. Rev. B*, 1975, **12**, 2111-2120.

6 J. P. Perdew, K. Burke and M. Ernzerhof, *Phys. Rev. Lett.*, 1996, **77**, 3865.

7 B. H. Lei, Z. H. Yang and S. L. Pan, *Chem. Commun.*, 2017, **53**, 2818-2821.

8 C. C. Jin, F. M. Li, B. L. Cheng, H. T. Qiu, Z. H. Yang, S. L. Pan and M. Mutailipu, *Angew. Chem. Int. Ed.*, 2022, **61**, e202203984.

9 Z. L. Chen, H. Zeng, D. D. Chu, F. F. Zhang, M. Cheng, Z. H. Yang and S. L. Pan, *Sci. China Mater.*, 2022, **65**, 2585-2590.

10 C. C. Jin, X. P. Shi, H. Zeng, S. J. Han, Z. Chen, Z. H. Yang, M. Mutailipu and S. L. Pan, *Angew. Chem. Int. Ed.*, 2021, **60**, 20469-20475.

11 Y. Dang, D. D. Chu, Z. H. Yang, H. S.Shi and S. L. Pan, *Inorg. Chem.*, 2022, **61**, 13600-13607.

12 M. K. Chaudhuri and B. Das, *Dalton Trans.*, 1988, 243–244.

13 S. Islamovic, B. Galic and M. Milos, *J. Enzym. Inhib. Med. Ch.*, 2014, **29**, 744–748.

14 Z. Q. Chen, F. M. Li, J. Han, Z. H. Yang, S. L. Pan and M. Mutailipu, *Chem. Commun.*, 2023, **59**, 2114-2117.

15 M. Q. Gai, Y. Wang, T. H. Tong, L. Y. Wang, Z. H. Yang, X. Zhou and S. L. Pan, *Chem. Commun.*, 2020, **56**, 3301-3304.

16 M. Cheng, C. C. Jin, W. Q. Jin and X. L. Hou, *Inorg. Chem.*, 2023, **62**, 9209-9216.

17 B. L. Cheng, W. J. Ma, A. Tudi, F. F. Zhang, Z. L. Chen, X. L. Hou, Z. H. Yang and S. L. Pan, *Chem. Mater.*, 2023, **35**, 5671-5679.

18 Z. Q. Chen, F. M. Li, Y. L. Liu, C. Cui and M. Mutailipu, *Inorg. Chem.*, 2023, **62**, 14512–14517.